Applied Catalysis B: Environmental 88 (2009) 213–223

Contents lists available at ScienceDirect

Applied Catalysis B: Environmental

journal homepage: www.elsevier.com/locate/apcatb

Kinetic and deactivation modelling of biphenyl liquid-phase hydrogenation over bimetallic Pt–Pd catalyst

Pedro Castaño, Daniël van Herk, Michiel T. Kreutzer, Jacob A. Moulijn, Michiel Makkee *

Delft University of Technology, Department of Chemical Engineering, Julianalaan 136, NL 2628 BL Delft, The Netherlands

ARTICLE INFO

Article history:
Received 7 August 2008
Received in revised form 24 September 2008
Accepted 26 September 2008
Available online 17 October 2008

Keywords:
Polycyclic-aromatic-hydrocarbon (PAH) hydrogenation
Noble metal catalyst
Bimetallic
Kinetic modelling
Sulphur poisoning
Biphenyl
Deactivation

ABSTRACT

The hydrogenation of biphenyl was modelled kinetically on a Pt–Pd supported catalyst, comprising the influence of the sulphur poisoning. Aromatic deep hydrogenation is one of the challenges for meeting the environmental requirements of fuels. Noble bimetallic catalysts are promising systems for such purpose due to their (i) improved activity compared to standard hydrotreating catalysts and their (ii) enhanced resistance toward sulphur poisoning in contrast to their monometallic counterparts. The experiments used for the modelling have been obtained in the intrinsic kinetic regime, excluding internal and external mass transfer limitations. A robust model for both kinetic and deactivation performance is derived, taking as initial estimations the values derived from the pseudo-first-order kinetics. This model clarifies the mechanisms of adsorption, reaction, and deactivation during polycyclic-aromatic-hydrocarbon (PAH) hydrogenation on intrinsic kinetic conditions.

1. Introduction

Polycyclic-aromatic-hydrocarbons (PAH) are hazardous compounds for the humans and environment [1]. They are present in several petrochemical feedstock, e.g. in diesel where their presence might give rise to the indirect formation of NO_x and the potential formation of particulate matter during combustion [2–4]. Furthermore, the higher amount of aromatics in diesel will give a lower cetane number [5] and thus, a drop in product quality. As a result, it is not surprising that environmental legislations in the future will demand a reduction of the maximum allowed amount of aromatics down to 10–15 vol.%, in the European Union and as it already occurred in Sweden with the so-called 'urban diesel 1' or 'class 1 diesel' containing 5 vol.% aromatics [6,7].

Hydrotreatment is the key process for upgrading refractory aromatic-rich streams in the oil refinery. The actual industrial units, however, have not been designed for reaching the extent of hydrodearomatization as set by the legislations [6,8,9]. Therefore, an intensification of the existing and future hydrotreaters is to be expected in the coming years [10]. Deep hydrodearomatization can only be achieved accounting (i) the development of more stable-active-selective catalysts, (ii) the improvement of the reactor design, and (iii) the enhancement of the understanding of the kinetic process.

Many authors considered noble-metal supported catalysts as candidates to revamp hydrotreaters [10–13], since they are far more active than the sulphided NiMo, CoMo or Ni catalysts, although they are more prone to sulphur poisoning. The stability of noble metal-supported catalyst (Pt) can be enhanced by incorporating a second metal (Pd) [14–21], although the stability is dependent on the preparation method [22]. The explanation of this stabilization effect is a transformation in the electronic state [18,23] or an inhibition of the metallic agglomeration [24]. The stability of the Pt–Pd supported catalysts makes these systems adequate for the final step of the deep desulphurization [25,26].

The kinetic modelling of aromatic gas-phase hydrogenation has been widely studied in the literature over a variety of catalysts [27,28] and the mechanisms have been elucidated [29,30]. On the contrary, polycyclic-aromatic liquid-phase hydrogenation has received less attention although this process will be more critical for the refineries [6,10]. In addition, the kinetic models for the liquid-phase hydrogenation have been mainly studied on Ni supported catalysts [31,32], whereas the noble metal supported catalysts would have a higher activity and stability towards sulphur poisoning (compared to Ni^0) [33].

Biphenyls are the by-products of the hydrodesulphurization of substituted dibenzothiophenes, and together with naphthalenes,

* Corresponding author. Tel.: +31 15 278 1391; fax: +31 15 278 5006.
E-mail address: m.makkee@tudelft.nl (M. Makkee).

0926-3373/$ – see front matter © 2008 Elsevier B.V. All rights reserved.
doi:10.1016/j.apcatb.2008.09.034

Nomenclature

c_s	total number of sulphur-molecules exposed to catalyst ($mol_{benzothiophene}$)
CN	cetane number
C_i	concentration of compound i ($mol\ L^{-1}$)
C_S	sulphur concentration (ppb)
C_i'	concentration of compound i at $(-r_i)_{max}$ ($mol_i\ L^{-1}$)
D_{eff}	effective diffusivity ($m^2\ h^{-1}$)
Dp	particle diameter (μm)
E_a	activation energy ($kJ\ mol^{-1}$)
k_i	kinetic constant of step i ($L^{1.5}\ (h\ g_{cat}\ mol_{H_2}^{0.5})^{-1}$)
K_i	adsorption constant of compound i ($L\ mol_i^{-1}$)
L	particle diffusion length, Dp/6 (m)
n_s	number of sample
N_{cat}	number of accessible metal moles (mol_{metal})
N_S	number of moles of sulphur-molecules (mol_S)
P_{H_2}	partial pressure of hydrogen (MPa)
r_i	rate of reaction ($mol_i\ (h\ L)^{-1}$)
$(r_i)_{max}$	maximum rate of disappearance-formation ($mol_i\ (h\ L)^{-1}$)
R	molar ratio of sulphur:accessible-metal (N_S/N_{cat})
SSR	sum of square residuals
t	time (h)
t_s	time of sampling
v_s	volume of sample withdrawal (1.5 mL $sample^{-1}$)
V, V_t	volume of liquid in the reactor, total volume of liquid seen by the catalyst (L)
W_C	weight of catalyst ($g_{cat\_}$)
X	conversion (%)

Greek letters

α_1, α_2	hydrogen order of reaction of first and second step of biphenyl hydrogenation
β	number of adsorption sites
γ	deactivation function
θ	rate of sampling ($L\ h^{-1}$)
κ_i	kinetic constant of step i ($mol_{BPH}\ (g_{cat}\ h)^{-1}$)
κ_i'	kinetic constant of step i (h^{-1})
λ	deactivation constant ($mol_{metal}\ mol_S$)
ξ_{ads}	adsorption term for a Langmuir–Hinshelwood type mechanism
τ	batch space time ($g_{cat}\ h\ mol_{BPH}^{-1}$)
Φ_{WP}	Weisz–Prater module

Subscripts

a, d	aging and deactivation
BCH	bicyclohexyl
BPH	biphenyl
cat	catalyst
CHB	cyclohexylbenzene
S	sulphur

they form the majority of the polycyclic-aromatic fraction in diesel fraction [8]. Fig. 1 shows the increase of the cetane number (CN), when biphenyl is hydrogenated stepwise using the correlations given elsewhere [34,35]. Considering the fact that this increase in CN also holds for the rest of aromatics contained in diesel, deep

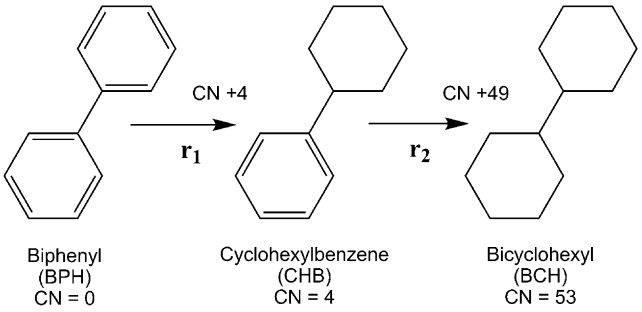

Fig. 1. Scheme of the reactions taking place during biphenyl hydrogenation and their influence on its individual cetane number (CN).

hydrogenation (full conversion) of aromatic-rich cuts as LCO (Light Cycle Oil, containing >70 wt.% of aromatics) into naphthenes are the key to upgrade such refractory feedstock.

In this work we study the hydrogenation of biphenyl on a supported bimetallic (Pt–Pd) catalyst in the liquid phase. Operating under the right conditions, we obtain data in the intrinsic kinetic controlled regime, excluding transport and hydrodynamic effects. The target is to develop a tool for a kinetic understanding of the deep aromatic hydrogenation over bimetallic supported catalyst. The mechanistic implication of the kinetic results and the modelling, both related with the catalyst properties (measured by different characterization techniques), are discussed. The model is then further elaborated by the incorporation of the effect of catalyst poisoning by sulphur and aging.

2. Experimental

2.1. Catalyst

The catalyst (0.1 wt.% Pt + 0.4 wt.% Pd/Al_2O_3) had been supplied by *Heraeus*, it was crushed and sieved in the ranges: 70 ± 20, 120 ± 30, and 200 ± 50 μm. Temperature programmed reduction (TPR) profiles of the fresh catalyst (results not displayed here) showed that the catalyst was originally in its reduced form and that some impurities were desorbed at 150 °C. Thus, the catalyst was pretreated *in situ* prior to the rest of analyses and kinetic measurements under the following conditions: atmospheric pressure; H_2 flow rate, 80 $cm^3\ min^{-1}$; heating up to 250 °C; isothermal reduction at that temperature for 4 h.

The metallic content of the catalyst was obtained by means of inductively coupled plasma (ICP-OES), PerkinElmer Optima 5300DV. The surface properties of the catalyst were determined by N_2 adsorption–desorption isotherms at −196 °C in a Quantachrome Autosorb-6B instrument, while the metallic properties were analyzed by CO adsorption isotherm at 35 °C in a Quantachrome Autosorb-1C apparatus. The sample was initially reduced following the same procedure described for the reaction plus the desorption under vacuum at 300 °C for 6 h. Transmission electron microscopy (TEM) was performed using a FEI Tecnai F20 electron microscope with a field emission gun (FEG) as the source of electrons operated at 200 kV. Samples were mounted on a Quantifoil® microgrid carbon polymer supported on a copper grid by placing a few droplets of a suspension of grounded sample in ethanol on the grid, followed by drying at ambient conditions.

2.2. Kinetic experiments

Aromatic hydrogenation experiments were carried out in a 0.3 L batch stirred reactor (Medimex Inc.). The first step consisted of loading 0.2–2.0 g of catalyst in the reaction system, followed by the

treatment described above. Then the liquid-reactive mixture was loaded into the reactor. After reaching a steady state of temperature and pressure, a hydrogen flow (in order to maintain a constant pressure) was allowed and the stirring system was turned on, representing the beginning of reaction. The concentration of reactants and products did not vary significantly during the steps prior to reaction.

The material of construction of the reactor was stainless steel 316. Including baffles, stirrer and walls, the total metallic area in contact with the liquid is ca. 2×10^{-2} m^2. The liquid mixture consisted with 0.15 L of tetradecane (Acros Organics, 99%) solution containing 4.41×10^{-2} mol L^{-1} of hexadecane (Merck, 99%) as a reference component and $6–25 \times 10^{-2}$ mol L^{-1} of aromatic-naphthenic compound(s) as reactant(s): biphenyl (solid, Acros Organics, 98%); cyclohexylbenzene (liquid, Acros Organics, 98%); bicyclohexyl (liquid, Aldrich, 99%). The initial concentrations of reactants and products were varied in order to study the effect of product inhibition on the kinetic expressions.

The operating conditions were; pressures, 2.5–6 MPa and temperatures, 120–150 °C. The analysis of the unreacted compounds and products were undertaken in a ChromPack CP9001 gas chromatograph equipped with a 50 m HP-1 column and a FID. In the analysis, the variation of injected volume was corrected using hexadecane as internal standard.

The influence of the catalyst deactivation on the kinetic mechanisms has been studied by means of using two feeds: (i) as it was originally prepared and (ii) treated with a pre-reduced adsorbing bed (extrudates of Ni–NiO/Al_2O_3, BASF, atmospheric pressure and 150 °C). The qualitative analysis of sulphur compounds was carried out by GC–MS using a Shimazu GCMS-QP2010 apparatus with a TRB-1MS column, whereas the quantitative concentration of sulphur was measured following the ASTM D 5453-03 standard.

2.3. Data processing and kinetic equations

The batch space time (τ) had been defined for comparing the performance of runs with different catalyst loading:

$$\tau = \left(\frac{W_C}{VC^0_{BPH}}\right)t \tag{1}$$

where V is the volume of the reaction (typically, 0.15 L), W_C the catalyst loading, C^0_{BPH} the initial concentration of byphenyl, and t is the time of reaction.

Many authors [36–38] have claimed that aromatic hydrogenation follows a pseudo-first-order kinetic model at low conversion level:

$$-\mathrm{Ln}(1-X) = \kappa_i \tau \tag{2}$$

where the kinetic constants κ_i can have two types of units: (i) $\mathrm{mol_{BPH}\ g^{-1}_{cat}\ h^{-1}}$ using τ; or (ii) h^{-1} (κ') using t. The conversion of double bounds (X) has been defined as

$$X = \frac{C_{BCH} + 0.5C_{CHB}}{C_{BPH} + C_{CHB} + C_{BCH}} \tag{3}$$

This definition gives values of the conversion over the entire range of operation, independently on the predominant stage of the hydrogenation (Fig. 1).

The hydrogen concentration in the liquid-phase (C_{H_2}) was calculated using the thermodynamic data from Refs. [39–41]. The concentration values were almost linearly dependent with the pressure and temperature in the regime studied (C_{H_2} = 0.10–0.35 mol L^{-1}), which assures a constant (hydrogen is constantly consumed during the reaction and supplied by the gas phase) molar ratio hydrogen:aromatic of 2–3.

The differential equations, according to a Langmuir–Hinshelwood type mechanism, that describe the kinetic model of biphenyl hydrogenation in the integral reactor, are the following:

$$\frac{dC_{BPH}}{dt} = -\left(\frac{W_C}{V-\theta t}\right)\frac{k_1 C_{BPH} C^{\alpha_1}_{H_2}}{\xi_{ads}}\gamma \tag{4}$$

$$\frac{dC_{CHB}}{dt} = \left(\frac{W_C}{V-\theta t}\right)\left(\frac{k_1 C_{BPH} C^{\alpha_1}_{H_2}}{\xi_{ads}} - \frac{k_2 C_{CHB} C^{\alpha_2}_{H_2}}{\xi_{ads}}\right)\gamma \tag{5}$$

$$\frac{dC_{BCH}}{dt} = \left(\frac{W_C}{V-\theta t}\right)\frac{k_2 C_{CHB} C^{\alpha_2}_{H_2}}{\xi_{ads}}\gamma \tag{6}$$

where θ (in L h^{-1}) is the rate of volume decrease caused by the sample withdrawal during reaction. θ represents a discrete series (experimentally) by the continuous function:

$$\theta = \frac{n_s|_i v_s}{t_s|_i} \tag{7}$$

where n_s is the number of the sample i, v_s the withdrawal volume per sample (1.5 mL sample^{-1}), and t_s is the time at which sample i was taken. It should be noted that the error could be introduced if the correction for the sampling withdrawal is not taken into account.

ξ_{ads} is the term of the product inhibition by adsorption of reactants and products and it could have two forms depending if the adsorption of the hydrogen-aromatic is non-competitive:

$$\xi_{ads} = (1 + K_{BPH}C_{BPH} + K_{CHB}C_{CHB} + K_{BCH}C_{BCH})\left(1 + \sqrt{K_{H_2}C_{H_2}}\right) \tag{8}$$

Or competitive:

$$\xi_{ads} = \left(1 + K_{BPH}C_{BPH} + K_{CHB}C_{CHB} + K_{BCH}C_{BCH} + \sqrt{K_{H_2}C_{H_2}}\right)^{\beta} \tag{9}$$

where the adsorption of hydrogen has been considered to be dissociative and β represents the number of sites implicated in the adsorption process. Non-competitive models suggest that the hydrogen is adsorbed and dissociated on a different metal- or on a support-site and then migrates along the surface until it reaches an aromatic molecule adsorbed on the metal-site where they react. On the other hand, competitive models assume that both hydrogen and the aromatic molecules compete for adsorption on the same metal sites where they react. An extensive model discrimination indicated that competitive models are more likely to occur in gas-phase hydrogenation over noble metal supported on alumina catalysts [30]. Table 1 summarizes the non-competitive models used for the kinetic modelling of biphenyl hydrogenation, each one corresponds to a different number of adsorption sites (β).

A simplistic way to rationalize the deactivation is that the sulphur-molecules (N_S, calculated using C_S) are in equilibrium with the accessible metal sites (N_{cat}, calculated using the values of W_C, metallic content of the catalyst from ICP and dispersion from CO chemisorption), and the deactivation function ($\gamma = -r_i/-r_{i0}$) has a linear dependency with the molar ratio between the amount of

Table 1
Models of deactivation used for fitting hydrogenation runs with treated and non-treated feedstock.

Model	β	Adsorption
1	0	No adsorption limited
2	1	1 site
3	2	2 sites

Table 2
Models of deactivation used for fitting hydrogenation runs with treated and non-treated feedstock.

Model	γ_d	γ_a	Type
4	1	1	No deactivation
5	Eq. (10)	1	Linear; $\gamma(R)$
6	Eq. (11)	1	Linear; $\gamma(t)$
7	Eq. (12)	1	Reciprocal
8	Eq. (13)	1	Exponential
9	Eq. (12)	Eq. (10)	Reciprocal × linear
10	Eq. (13)	Eq. (10)	Exponential × linear

sulphur-molecules exposed per accessible metal site ($R = N_S/N_{cat}$), note that R is proportional to the time-on-stream in a continuous trickle-bed reactor:

$$\gamma = 1 - \lambda R \tag{10}$$

One might expect that the deactivation function depends on contact time catalyst-feed instead of R (note that R is proportional to the time-on-stream in a continuous trickle-bed reactor):

$$\gamma = 1 - \lambda t \tag{11}$$

The poisoning of metal sites by sulphur had been reported to be non-linear or, more precisely, selective [42,43]. These models are based on a distribution of the activity, from where the most active sites deactivate faster. The equations for modelling deactivation can be summarized as reciprocal or exponential [44]:

$$\gamma = \frac{1}{1 + \lambda R} \tag{12}$$

$$\gamma = e^{-\lambda R} \tag{13}$$

In long-term catalyst decay, the profile can be divided into a deactivation (γ_d) and aging (γ_a) function [45]:

$$\gamma = \gamma_d \cdot \gamma_a \tag{14}$$

In the reactor used, the contact time is relatively short (ca. 3 h) and we assume that the poisoning occurs before the beginning of the kinetic run and no deactivation takes place within each run, allowing further deactivation via aging. On the basis of these criteria we proposed the six models (numbered 4–10 after the models without deactivation, see Table 1) of the kinetics with deactivation as summarized in Table 2.

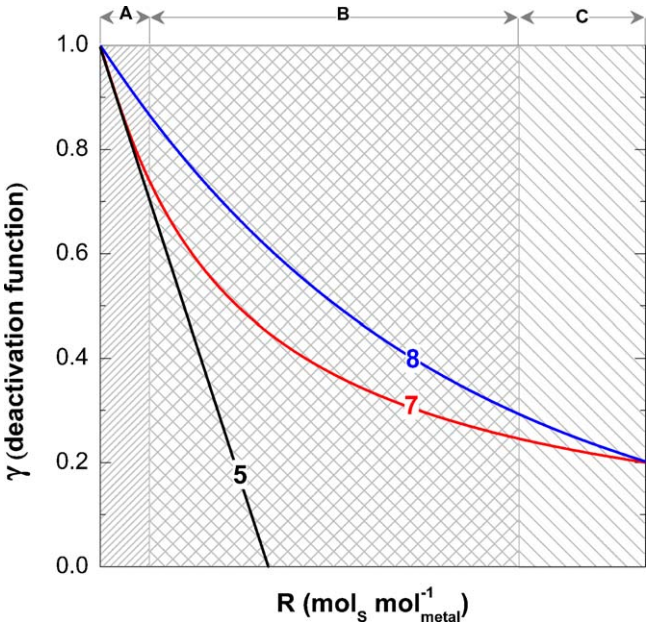

Fig. 2. Example of deactivation function (models 5, 7 and 8, Table 2) along the molar ratio exposed-sulphur:accessible-metal-site (R).

Fig. 2 shows an example of arbitrary deactivation profiles with the same initial and final value of γ, using the models 5, 7 and 8 summarized in Table 2, note that model 6 is not a function of R and cannot be represented in this graph.

It is important to note (see Fig. 2) that the models with reciprocal deactivation (models 7 and 9) predict more selective deactivation as compared to exponential ones (models 8 and 10), when the final deactivation is fixed. This conclusion is distilled for the faster initial deactivation of models 7 and 9 as compared to models 8 and 10 correspondingly when a final activity is fixed (Fig. 2).

From Fig. 2, three regions can be delineated: (A) linear deactivation is predominant at low values of R and thus model 5 would predict better the experimental results, (B) models 7 and 8 (with the minimum number of constants) can model the change in the deactivation mechanism from the deactivation towards aging, (C) at greater values of R, models 9 and 10 would be more realistic since aging is dominant at this stage, the difference between models 5 and 6 is that the former depends on the amount of poisoning seen by the catalyst (R) while the latter depends on the time of contact (slope = 0 in Fig. 2), which can be linked with fouling of coke. Note that industrial reactors used for hydrogenation of polycyclic-aromatics (trickle beds) normally operate under the aging regime (C); in this case the activity decay during operation (to retain activity normally the temperature is raised over the years).

In order to account for the effect of the temperature, the kinetic (k_i) and adsorption (K_i) constants represented in Eqs. (4)–(6) have been reparameterizated by the Arrhenius and Van 't Hoff equations, respectively.

The differential equations (Eqs. (4)–(6)) have been solved with Matlab™; minimizing the sum of squared residuals (SSR) using the large-scale algorithm, subspace trust region method based on the interior-reflective Newton method:

$$SSR = \sum_{i=1}^{N_{exp}} [C_i|_{calc}(k_1, k_2, K_{BPH}, \ldots) - C_i|_{exp}]^2 \tag{15}$$

3. Results

3.1. Catalyst and feedstock properties

The properties of the catalyst were: Pt content, 0.10 ± 0.01 wt.%; Pd content, 0.39 ± 0.01 wt.%; BET surface area, 115 $m^2\ g^{-1}$; total pore volume, 0.61 $cm^3\ g^{-1}$; micropore volume, 0.004 $cm^3\ g^{-1}$; average mesopore diameter, 20 nm; metallic area, 4.8 ± 0.4 $m^2\ g^{-1}$; metallic dispersion, 37 ± 1%; average metal-particle size based on CO adsorption, 8 nm. The average metal-particle size was also confirmed by TEM microscopy, as it is shown in Fig. 3.

Upon comparing the TEM micrographs of the deactivated and fresh catalyst, we concluded that the metal-particles do not agglomerate during on-stream operation due to the stabilization effect of Pd on Pt [23] and the relatively mild operating conditions used (130–150 °C). Besides, energy dispersive X-ray (EDX) analysis on metallic particles showed that Pt and Pd phases coexist within the same particles, hence the advantages of bimetallic catalyst were assured.

According to GC–MS analysis, sulphur was present in feedstock (particularly in the solvent; tetradecane) as benzothiophene. The quantitative concentrations of benzothiophene (measured by ASTM D 5453-03) in the feeds were the following: (i) untreated feedstock, C_S = 638 ± 12 ppb; (ii) treated feedstock, C_S = 19.4 ± 0.1 ppb; (iii) liquid by-product (after a kinetic run of treated feedstock), C_S < 3 ppb.

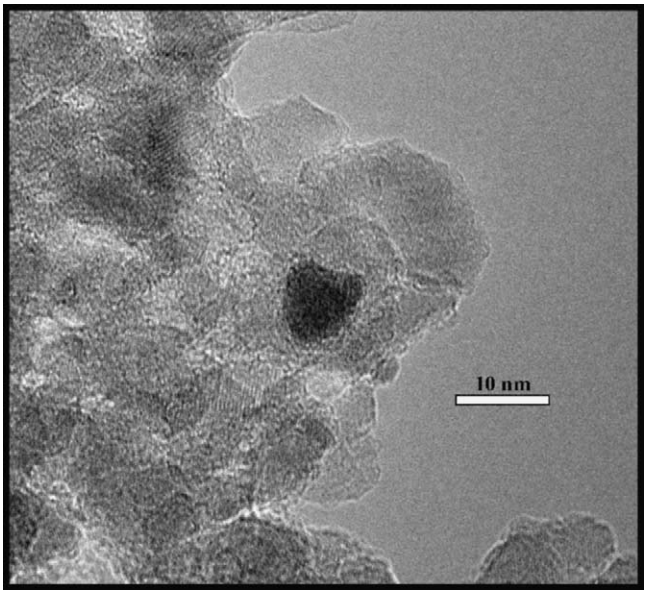

Fig. 3. TEM micrograph of a bimetallic Pt–Pd particle on the alumina support.

3.2. Apparent kinetics, deactivation and mass transfer

The hydrogenation of biphenyl (BPH) produces cyclohexylbenzene (CHB) and bicyclohexyl (BCH). No other liquid by-product was detected in the reactor at the studied reaction conditions. Six examples of reaction performances are shown in Fig. 4, all of them demonstrate experimentally the applicability of the scheme represented in Fig. 1: biphenyl hydrogenates in two steps, where k_1 and k_2 are the kinetic constants of each hydrogenation step; r_1 and r_2, respectively. In the case of untreated feedstock (Fig. 4(a)), at low conversion an induction period is observed at $C_{BPH} > 7.0 \times 10^{-2}$ mol L^{-1}, in agreement with other authors [18,30]. However, this effect is not shown for the treated feedstock (Fig. 4(b)–(f)) even with a total aromatic concentration of 2.3×10^{-1} mol L^{-1} (Fig. 4(b)). The induction period is then ascribed to the removal of non-equilibrated sulphur species from the catalyst, in other words, the occurrence of a maximum in the concentration of sulphur at the catalyst surface at the beginning of the reaction (during stabilization time) which is eliminated to a certain extent during hydrogenation of aromatics.

The concentration of cyclohexylbenzene exhibits a maximum that is (i) approximately independent of temperature and pressure, and (ii) appears at lower batch space-time values when temperature is increased (see Fig. 4(c) and (d)). This result can be explained by the fact that the activation energies of both steps (E_{a1} and E_{a2}) have similar values.

Upon comparing the slope of disappearance of biphenyl and cyclohexylbenzene in Fig. 4, it is tentatively concluded that the hydrogenation rate of the first step is faster than that of the second step, particularly when the benzothiophene is virtually eliminated from the feed (all graphs of Fig. 4 except (a)).

The effect of hydrogen partial pressure on the selectivity can be seen upon comparing the results presented in Fig. 4(d)–(f). At higher temperatures, the increase of hydrogen partial pressure does not change the shape of the concentration profiles, nevertheless both reaction steps are accelerated. This result indicates that the reaction orders of hydrogen (α_1 and α_2) are positive.

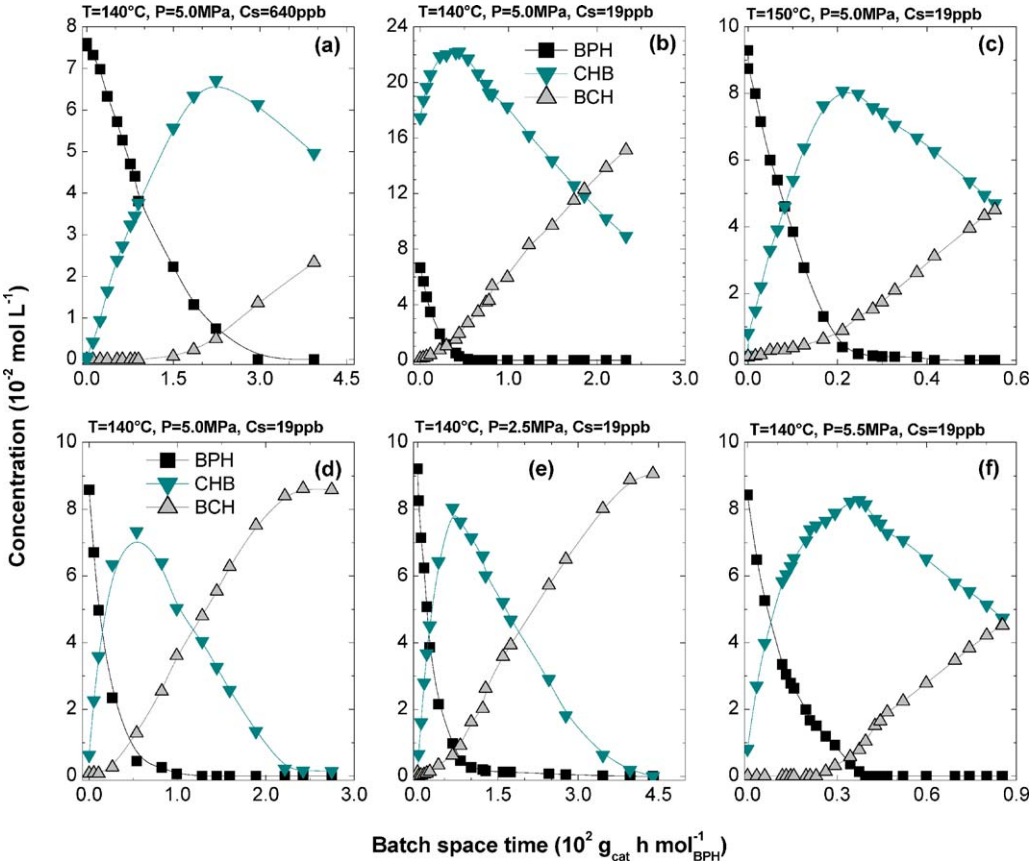

Fig. 4. Concentration profile of reactants and products during biphenyl-cyclohexylbenzene hydrogenation at the conditions displayed in the titles. Each run (a–f) corresponds to the conditions described in the titles.

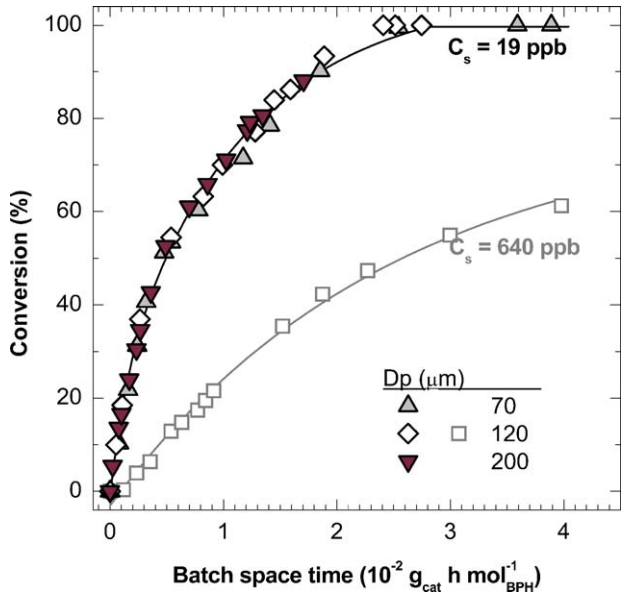

Fig. 5. Conversion profile of (a) treated, W_C = 0.4–0.6 g_{cat}; and (b) untreated feedstock, W_C = 1.62 g_{cat}. Conditions: 140 °C, 5 MPa.

The use of different feeds and catalyst loadings enabled us to study the effect of deactivation on the kinetic model. Fig. 5 shows the biphenyl conversion profile along the batch space-time of the two feedstock at the same reaction conditions. We assumed that the sulphur-molecules poisoned the active sites during the initial contact time feedstock-catalyst (before reaction, needed for temperature ramp and stabilization time) and then an equilibrium between the adsorbed and non-adsorbed species is established as demonstrated by the result of sulphur concentration in the liquid by-product, after reaction.

The importance of the external and internal mass transfer limitations was evaluated by several methodologies, using the kinetic results of the treated feedstock.

Fig. 6 represents the reciprocal kinetic constant values, calculated using Eq. (2) and using t instead of τ versus the inverse of the catalyst loading. The linear dependency displayed in Fig. 6 evidences that the external mass transfer could be neglected [46]. Moreover, the use of different stirring rates did not affect the activity of the catalyst in the range studied (900–1500 rpm), results not displayed here.

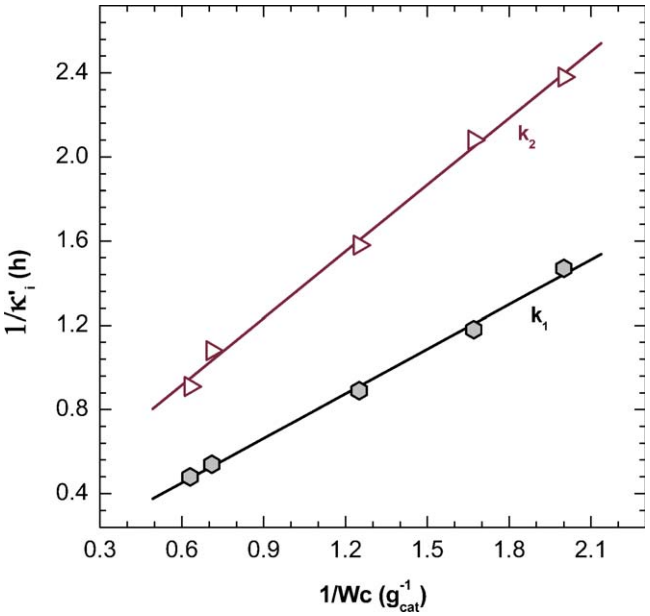

Fig. 6. Effect of the catalyst loading (W_C) on reaction rate (κ'_i). Conditions: 140 °C, 5 MPa.

The possible internal mass transfer limitations were investigated by (i) varying the particle diameter in the ranges described in Section 2 and (ii) calculating the Weisz–Prater module (Φ_{WP}). In Fig. 5 the results ascribed as C_S = 19 ppb correspond to three different particle sizes; the identical hydrogenation performance of these three catalysts demonstrates the absence of internal mass-transfer limitations.

For a first-order kinetics, the Weisz–Prater module can be calculated as follows:

$$\Phi_{WP} = \frac{(-r_i)_{max} L^2}{D_{eff} C'_i} < 0.15 \quad (16)$$

where C'_i is the concentration of i (i = BCH, CHB) at the maximum rate of the disappearance-formation of each compound; $(-r_i)_{max}$, while the effective diffusivity (D_{eff}) was derived from the Wilke–Chang equation multiplied by the porosity over the tortuosity. The values of Φ_{WP} at the maximum rates are 0.071 and 0.028 for the first and second step of hydrogenation, respectively. The Φ_{WP} for hydrogen resulted in values one or two order of magnitude lower than these of the hydrogenation of biphenyl and cyclohexylbenzene due to the smaller kinetic diameter of hydrogen in respect to the aromatic molecules. Considering that the value of Φ_{WP} for exclusion of the internal mass-transfer limitations is 0.15, we can conclude that the intra-particle resistance is negligible in comparison with the reaction resistance, under the applied operating conditions.

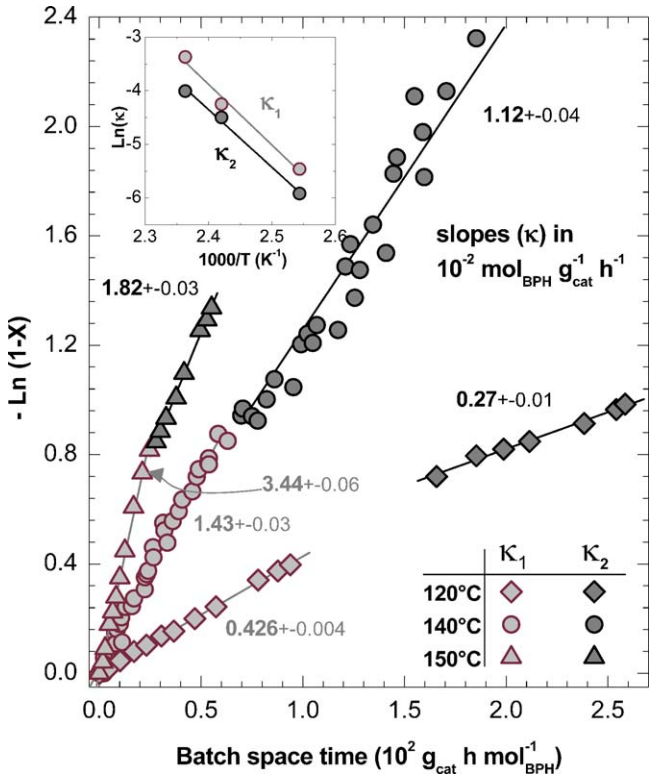

Fig. 7. Influence of the temperature on the pseudo-first kinetic plots during the biphenyl hydrogenation at 5 MPa.

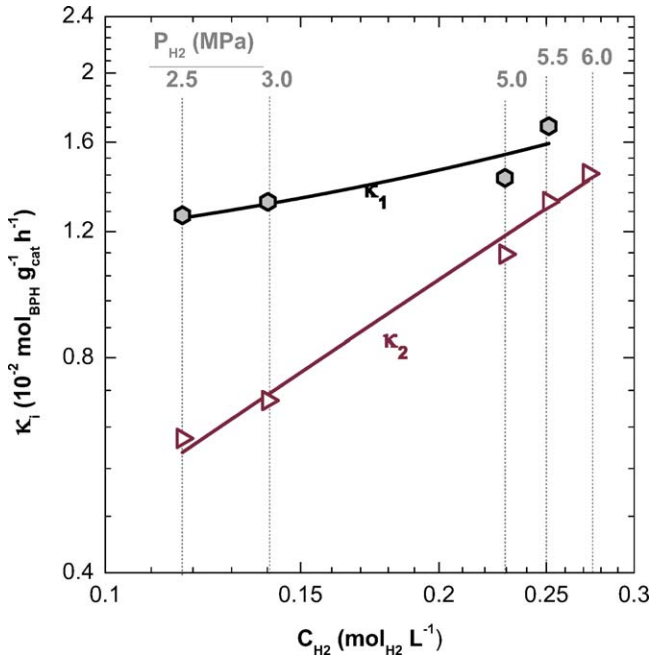

Fig. 8. Influence of the hydrogen concentration in the liquid phase on the pseudo-first kinetic constant of biphenyl (κ_1) and cyclohexylbenzene (κ_2) hydrogenation at 140 °C.

3.3. Intrinsic kinetic data

Based on the experiments and generally accepted criteria on the exclusion of the deactivation and the internal–external mass transfer limitations, we were able to collect data in the intrinsic kinetic regime.

Fig. 7 displays the temperature dependency of the catalytic activity; κ values of Eq. (2) and the Arrhenius plots of such calculated constants (sub-graph in Fig. 7). The representation of pseudo-first-order kinetic plot shows a discontinuity caused by a change in the dominant mechanism: (i) initial region κ_1, biphenyl to cyclohexylbenzene and (ii) secondary region κ_2, cyclohexylbenzene to biclyclohexyl. The Arrhenius plots of κ_1 and κ_2 resulted in activation energies; $E_{a1} = 94 \pm 11$ kJ mol^{-1} and $E_{a2} = 89 \pm 6$ kJ mol^{-1}, respectively. These values have been used as initial estimations of E_{a1} and E_{a2} and they corresponded to a scenario free of mass transfer resistances [32].

The influence of the hydrogen concentration in the liquid phase (C_{H_2}) on the kinetic constants (κ_1 and κ_2) is shown in Fig. 8. By the logarithmic representation we calculate the reaction order of hydrogen by estimating the slopes; $\alpha_1 = 0.3 \pm 0.1$ and $\alpha_2 = 1.01 \pm 0.06$. These values were used as initial estimations for the modelling and we should consider that these values have been obtained assuming pseudo-first-order kinetics as well as no adsorption term (ξ).

The increase of the hydrogen partial pressure causes an increase in catalytic activity for both steps of the sequential hydrogenation (Fig. 8). Thus, the hydrogen did not compete for the adsorption against the aromatic molecules in the applied reaction conditions, due to the relative low concentration of the aromatics in the liquid phase. As a consequence the adsorption constant for hydrogen (K_{H_2}) can be neglected in our experimental conditions, resulting in the simplification of Eqs. (8) and (9):

$$\xi_{ads} = (1 + K_{BPH}C_{BPH} + K_{CHB}C_{CHB} + K_{BCH}C_{BCH})^{\beta} \quad (17)$$

4. Discussion

Measuring intrinsic kinetics enabled us to propose models based on the Langmuir–Hinshelwood mechanisms based on the scheme of Fig. 1 and Eqs. (4)–(6). We divided the models in the ones assuming either negligible or significant deactivation.

For the modelling three different approaches can be pursued, which in an increasing order of complexity are (i) differential reactor (initial rate), (ii) pseudo-first-order kinetics and (iii) integral reactor. As the complexity is increased so does the accuracy [47]. The use of differential reactor is a useful tool for comparing catalytic performances. Pseudo-first-order kinetics are easy to fit but the interpretation of the results must be taken with care, since side-effects can be responsible for some observations. In this work pseudo-first-order kinetics have been used to assess assumptions and to obtain initial estimations for the integral model. The kinetic understanding is, consequently, much more precise using integral models, particularly for processes such as deep-hydrodearomatization where high conversions should be modelled.

The difference in reaction orders of hydrogen (α_1 and α_2, Fig. 8), combined with the different kinetic performance of each step (κ_1 and κ_2, Fig. 7), indicated that the performance in the hydrogenation of a single aromatic-ring strongly depends on the contiguous (aromatic or naphthenic) group. In the case of naphthalene this is more coherent as both electronic resonances (from each ring) interact with each other. We should notice, however, that biphenyl also shows this kind of behaviour and each hydrogenation step is an independent reaction.

Interestingly, the ratio of the accessible-metal-atom/sulphur-molecule (inverse to R value) were in the range 20–40 and 500–1200 for the untreated and treated feedstock, respectively, indicating that the effect of sulphur can be probably neglected by using the treated feedstock. The initial rate of hydrogenation in both treated and untreated feedstock can be calculated from the kinetic performance as displayed in Fig. 5; in this example the rate decreases by a factor of 5.8 from the original activity, whereas the

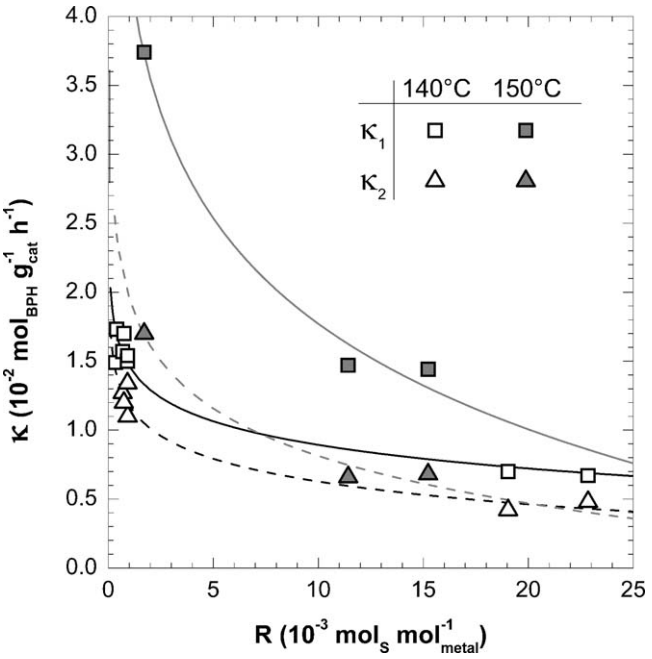

Fig. 9. Deactivation profiles of both hydrogenation rates κ_1 and κ_2 as a function of the molar ratio sulphur:metal. The plotted lines are present to guide the eye, no model involved. Conditions: 5 MPa.

relative accessible-metal-atom/sulphur-molecule ratio was around 20–40.

Several deactivation profiles (representative of all experimental trends) are shown in Fig. 9 using 140 and 150 °C as the reaction temperature, where the decay of the kinetic constants (κ_1 and κ_2) has been traced along the ratio sulphur:metal (R) described in Section 2.3. The profiles shown in Fig. 9 demonstrate that the deactivation is selective and, therefore, certain active sites of the catalyst deactivated faster than other sites. Though, it is impossible to conclude from Fig. 9 which type of deactivation mechanism is most predominant, and should be explained by reciprocal or exponential models.

The deactivation profiles of κ_1 and κ_2 at 140 °C vary only in the initial ($R = 0$) activity, whereas at 150 °C the profiles are different. This result and the fact that the difference in temperature is small (10 °C), indicate that the stabilization period has not been reached using temperatures of 150 °C and lower R values; consequently the measured activity at these conditions is higher than expected. Moreover, our experimental setup allows to obtain kinetic result of both deactivation and non-deactivation regime, decoupling the decay of κ_1 and κ_2 at the same time. This is true if we assume that the sulphur species are in equilibrium with the metal sites at the beginning of the reaction.

The sulphur molecules can deactivate the catalyst by three different mechanisms [48]: (i) PtS–PdS formation, (ii) adsorption of H_2S on the active sites (generated by desulphurization of the benzothiophene) or (iii) metallic particle growth (sintering of the active site). The PtS–PdS formation is not likely under our reaction conditions [48]. The TEM micrographs of the fresh and deactivated catalyst lead to conclude that no particle growth is observed. Thus, the site blocking by the adsorption of benzothiophene seemed the most possible mechanism of deactivation.

The values of E_{a1}, E_{a2}, α_1, and α_2 reported in Figs. 7 and 8 were considered as initial estimations, but not as fixed parameters since we used more experiments for the modelling that these used for the previously mentioned figures. Besides, Figs. 7 and 8 use the correlations for the calculation of the batch space time (Eq. (1)), kinetic constant (Eq. (2)) and conversion (Eq. (3)), while for the modelling just the concentration of compounds (C_i) and the mass of catalyst (W_C) were used. The results presented in Figs. 4, 7 and 8 are the basic assumptions, e.g. the effect of the hydrogen adsorption has been neglected ($K_{H_2} = 0$) according to our experimental observations as discussed with Fig. 8.

4.1. Kinetic models with negligible deactivation

In the regime where the deactivation can be neglected, 210 data points (11 autoclave runs) were obtained. Three models were derived from Eqs. (4)–(6) and Eq. (17), giving different values of β and making several assumptions that can be summarized as follows:

I. $\alpha_i = 0.5$; the values calculated from Fig. 8 ($\alpha_1 = 0.3$ and $\alpha_2 = 1.0$) were used as initial estimations. Then, based on the trend of the results and pursuing the physical meaning of the constants, the values of both α_1 and α_2 were fixed to 0.5.
II. $\beta = 0$ (model 1), non-limited by adsorption; $\beta = 1$ (model 2), one adsorption site; $\beta = 2$ (model 3), two adsorption sites.
III. $\gamma = 1$; no deactivation.
IV. $K_{H_2} = 0$; based on the results displayed in Fig. 8.
V. $K_{BCH} = 0$; based on the initial fitting results K_{BCH} was in all cases 1–2 orders of magnitude lower than K_{CHB} or K_{BPH}.
VI. K_i values are independent of temperature. The heats of adsorption derived from the Van 't Hoff equation were within the error with values of 4–8 kJ mol^{-1} and large confidence intervals, i.e. there is only a very small influence of the temperature on the adsorption parameters. These results can be explained accounting the relatively small window of the studied temperatures and the high surface coverage of the aromatic-species that is associated with the liquid-phase reactions [49,50].

The estimated kinetic parameters of the three models based on the mentioned assumptions are summarized in Table 3 with 95% confidence intervals. As it was previously discussed in qualitatively terms with Fig. 4, the first step of the hydrogenation is around one order of magnitude faster than that of the second step. The higher activation energy of the former step (in models 2 and 3), however, should allow obtaining identical rates at higher temperatures.

The difference in the final results of α (assumption I) with these presented in Fig. 8, points that pseudo-first-order kinetics are not able to predict reaction orders accurately, and the results of Fig. 8 should be regarded as 'apparent'. The activation energies distilled form pseudo-first-order kinetics (Fig. 7) are comparable with the final results (Table 3).

According to the SSR results the best fitting corresponds to model 2 ($\beta = 1$) which has higher accuracy than that of model 3 ($\beta = 2$) with the same number of constants. This result points out that the mechanism of biphenyl adsorption involves one active site, whereas the kinetic models for naphthalene and tetralin for Ni^0 supported catalyst claimed to have two adsorption sites [31,51]. Two reasons can explain this one-site observation: (i) the lower steric hindrance of naphthalene compared to that of biphenyl to be absorbed using its two aromatic rings simultaneously, and (ii) the smaller size of the Pt–Pd particle as compared to that of bulky-Ni (15–20 wt.% Ni/Al_2O_3 typically used).

As seen in Table 3 the biphenyl adsorption constant (K_{BPH}) is ca. 5 times higher than that of the cyclohexylbenzene (K_{CHB}). Hence we assumed that both aromatic-rings of biphenyl are interacting

Table 3
Summary of the fitting results of the kinetic models used in the negligible deactivation regime.

	Model		
	1 ($\beta = 0$; SSR = 7.31×10^{-2})	2 ($\beta = 1$; SSR = 1.39×10^{-2})	3 ($\beta = 2$; SSR = 1.56×10^{-2})
k_1[a]	1.19 ± 0.04	19.5 ± 0.5	8.52 ± 0.07
E_{a1}[b]	99.8 ± 5.6	96.3 ± 2.2	96.4 ± 2.2
k_2[a]	0.106 ± 0.002	0.822 ± 0.025	0.381 ± 0.009
E_{a2}[b]	110 ± 12	85.3 ± 4.3	85.7 ± 4.3
K_{BPH}[c]		283 ± 11	29.2 ± 0.4
K_{CHB}[c]		49.6 ± 2.0	6.18 ± 0.17

[a] Values at 140 °C, units of k in $L^{1.5}$ (h g_{cat} $mol_{H_2}^{0.5})^{-1}$.
[b] Units of E_a in kJ mol^{-1}.
[c] Units of K in L mol^{-1}.

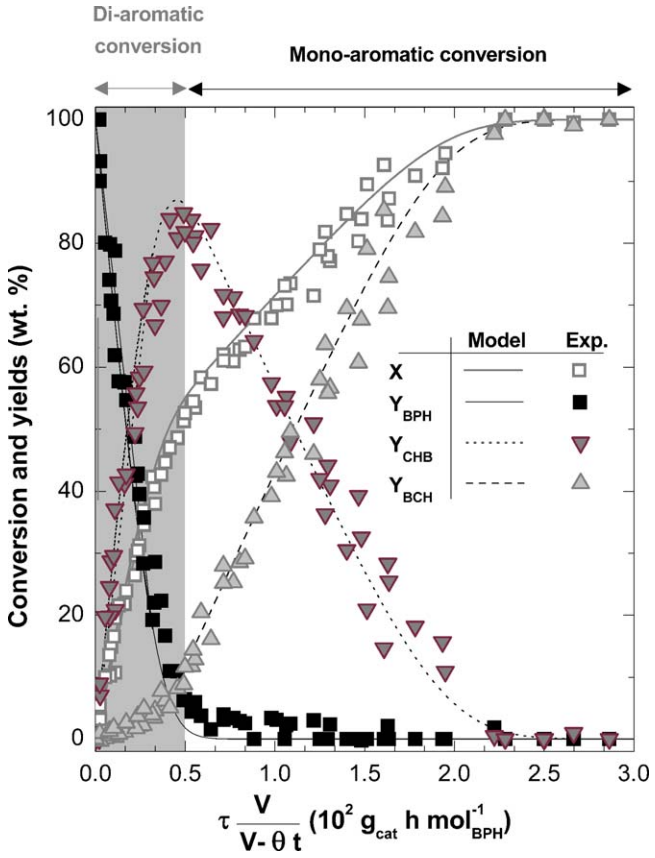

Fig. 10. Comparison of the predicted (lines) and experimental (points) values of the conversion and yields along the batch space time (corrected for the withdrawing rate) during biphenyl hydrogenation at 140 °C, 5 MPa and C_S = 19 ppb.

with the bimetallic clusters and no additional steric hindrance is expected for biphenyl as compared to that of naphthalene. Therefore, we concluded that the small size of the metal particles (<10 nm, from Fig. 3) is responsible for a change in the adsorption mechanism of the aromatics.

The results of the fitting of model 2 (best model for non-deactivation regime) are compared to experimental results in Fig. 10 in terms of the conversion and yields using a set of conditions as in the example: 140 °C and 5 MPa. The values of space time (τ) are corrected in Fig. 10 for the withdrawing rate (θ), see Eq. (1). As it is shown in Fig. 10 the model predicts a catalyst activity with high accuracy, as it is shown in Fig. 10. The plotted simulation in Fig. 10 corresponds to a sampling rate of 12 samples per hour, typical value of θ.

4.2. Kinetic models with significant deactivation

Using all the experiments for the modelling, obtained in both the negligible or significant deactivation regime, 293 data points (17 autoclave runs) were available. Using the same assumptions I, IV and V described in Section 4.1 (α_i = 0.5, K_{H_2} = 0 and the values of adsorption (K_i) were independent of temperature), we proposed seven models (Table 2) changing two hypotheses and adding an extra one:

II. $\beta = 1$; best fit consistent with negligible deactivation modelling.
III. $\gamma \neq 1$; seven models represented in Table 2.
VII. On the basis of the relatively small temperature window and the results of the heat of adsorption for K_i; we assumed that the catalyst deactivation constants (λ) were independent of the temperature
VIII. The deactivation by sulphur is faster than and occurs prior to reaction.

Table 4 summarizes the fitting results of the kinetic models proposed. According to the SSR values; the most robust model for predicting kinetics and deactivation under short-aging regime (A + B in Fig. 2) is model 7 (reciprocal). Therefore, the poisoning of the active sites is highly selective and the relative range of activity of sites is broad. These results are due to the fact that reciprocal model (7) predict more selective deactivation than exponential model one (8), as seen in Fig. 2. Considering the experimental observations shown in Fig. 9 (from where we derive the deactivation models), the majority of the data correspond to the non-selective and deactivation regime (A + B in Fig. 2), whereas the information regarding the aging period is limited. As a result, the most robust model for all the conditions including aging (A + B + C in Fig. 2) is an extension of model 7 (reciprocal); model 9 (reciprocal × linear). The low values aging constants (λ_a) of models 9 and 10 (Table 4) indicate that further experimentation is required for obtaining data regarding the aging process, which is particularly relevant for industrial and long-term operation in industrial reactors [45].

Fig. 11 shows the comparison between the experimental results (points) and the predicted values of model 7 (lines) at different condition, and in terms of aromatic reduction. The model satisfactorily predicts the experimental observations in the regime

Table 4
Summary of results in the fitting of the kinetic models used in the significant deactivation regime.

	Model						
	4 (SSR = 16.4 × 10^{-2})	5 (SSR = 5.32 × 10^{-2})	6 (SSR = 25.5 × 10^{-2})	7 (SSR = 2.38 × 10^{-2})	8 (SSR = 3.06 × 10^{-2})	9 (SSR = 2.38 × 10^{-2})	10 (SSR = 3.06 × 10^{-2})
k_1[a]	1.46 ± 0.17	6.76 ± 0.74	−0.111 ± 0.001	15.5 ± 1.4	10.9 ± 1.0	15.8 ± 1.5	10.8 ± 1.0
E_{a1}[b]	78.8 ± 5.9	80.4 ± 2.9	118 ± 11	99.1 ± 1.8	92.6 ± 2.1	99.5 ± 1.9	92.5 ± 2.1
k_2[a]	0.157 ± 0.011	0.40 ± 0.03	0.0141 ± 0.0010	0.74 ± 0.05	0.555 ± 0.038	0.757 ± 0.056	0.551 ± 0.037
E_{a2}[b]	37.8 ± 5.8	73.7 ± 4.0	70.5 ± 7.4	117 ± 3	103 ± 4	117 ± 3	104 ± 4
K_{BPH}[c]	9.02 ± 3.51	90.5 ± 12.9	−5.31 ± 0.44	172 ± 18	137 ± 15	174 ± 18	135 ± 16
K_{CHB}[c]	4.53 ± 0.94	19.7 ± 2.1	26.2 ± 5.4	37.6 ± 3.3	29.2 ± 2.6	37.9 ± 3.4	28.9 ± 2.6
λ_d[d]		29.5 ± 0.3	16.9 ± 1.8[e]	217 ± 0	70.8 ± 1.5	234 ± 23	70.8 ± 4.2
λ_a[d]						1.2 × 10^{-5} ± 3.2	1.1 × 10^{-6} ± 2.3

[a] Values at 140 °C, units of k in $L^{1.5}$ (h g_{cat} $mol_{H_2}^{0.5})^{-1}$.
[b] Units of E_a in kJ mol^{-1}.
[c] Units of K in L mol^{-1}.
[d] Units of λ in mol_{metal} mol_S.
[e] Units of λ for model 6 in h^{-1}.

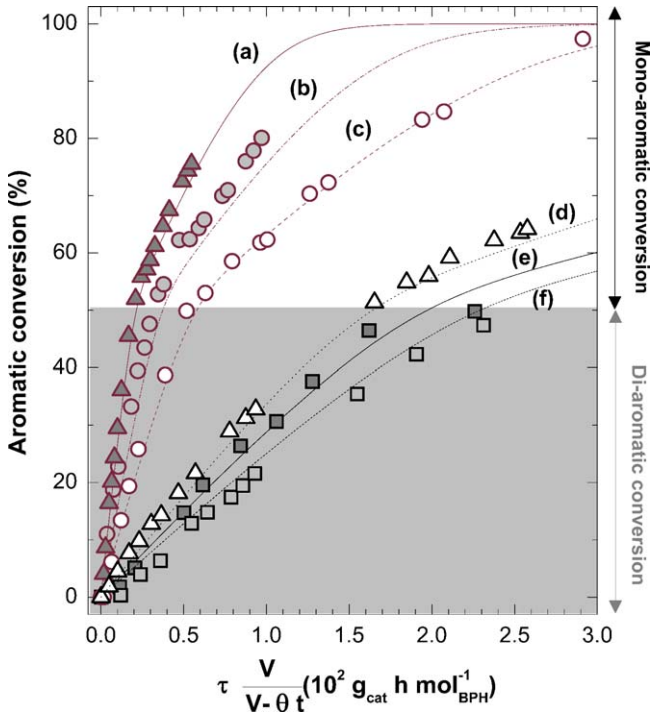

Fig. 11. Comparison between the aromatic conversion profiles during experimental runs (points) and predicted values from the model 7 (lines). Conditions of temperature (°C), pressure (MPa), sulphur (ppb), number of runs: (a) 150, 5.0, 19, 1; (b) 140, 5.0, 19, 1; (c) 140, 2.5, 19, 1; (d) 120, 5.0, 19, 1; (e) 140, 5.0, 640, 3; (f) 140, 5.0, 640, 4.

studied, in addition to changes in temperature, pressure, and deactivation. So it is a powerful tool for scaling-up and -down trickle beds.

Assumption VII was validated by means of fitting several deactivation + aging functions dependent on the time-on-stream, e.g. model 6 which is presented in Table 2. Comparing the fitting results of models 5 and 6, it is evident that using *t* instead of *R* in the deactivation functions has a negative effect on the accuracy of the model (SSR in Table 2). We also modelled similar deactivation equations of models 7 and 8 using the same approach and obtaining always higher SSR values (3 times higher than their non-time-dependent counterparts), results not presented here.

Models 2 and 4 are identical, except for the fact that more experiments had been used for the fitting of the latter. Comparing the values of their constants in Tables 3 and 4, we observed that the kinetic constants at 140 °C and the adsorption constants change appreciably while the activation energy decreases severely. This is due to the fact that the bulk of the experiments with negligible deactivation had been performed at 140 °C, while the experiments with deactivation had been performed at 150 °C. As a result, the fitting routine reduces the activation energy to minimize the error.

The adsorption constants, calculated for all the models and summarized in Tables 3 and 4 (also for K_{CHB}, not presented in these tables), increase exponentially with the number of rings present in the aromatic molecule. Hence, the adsorption strength of biphenyl cannot be calculated by adding the values of two cyclohexylbenzene molecules. This result has implications on the process design for deep-hydrodearomatization; we advise that feeds with highly polycyclic-aromatic content are pre-treated with a non-noble metal supported catalyst (e.g. Ni/Al_2O_3), followed by a bimetallic Pt–Pd supported catalyst in a second stage to achieve deep dearomatzation. Otherwise noble metallic sites are blocked by reactants, losing activity of more expensive Pt–Pd sites as compared to Ni ones.

5. Conclusions

The use of bimetallic Pt–Pd catalyst can overcome most of the problems associated with the use of noble-metal supported catalyst. For industrial application of such catalysts, kinetic models with mechanistic insights are required.

A kinetic model for the hydrogenation of biphenyl over bimetallic Pt–Pd catalyst is derived from experiments with and without negligible sulphur poisoning. Performing the experiments in a slurry-type reactor and on the basis of a set of conditions without mass transfer resistances: pressures, 2.5–6 MPa, temperatures, 120–150 °C, particle sizes <200 μm, stirring rates >900 rpm.

Pseudo-fist-order kinetic approach is used to make approximations and to obtain initial estimations of parameters. It has been demonstrated that using this methodology can induce error in the calculation of the order of reaction respect to hydrogen (α_i).

Biphenyl is adsorbed on the catalyst surface 5 times more strongly than its monoaromatic counterpart (cyclohexylbenzene), but the former reacts 10 times faster than the latter. The adsorption of reactants (biphenyl in particular) is non-competitive against the dissociative-adsorption of hydrogen and used only one site. The latter results can be explained taking into account the relatively small metal-particle size (<10 nm), whose curvature hinders the usage of two sites per aromatic adsorption.

The most robust model for predicting kinetics and deactivation under short-aging regime (A + B in Fig. 2) is model 7 (reciprocal deactivation), while the best model for long-aging regime (A + B + C in Fig. 2) is 9 (reciprocal deactivation + linear aging). However, the applicability of the latter is limited since further experimentation is required for calculating aging parameters (λ_a) more precisely. The implication of a reciprocal-deactivation model is that the distribution of activity among sites is quite broad and the most active sites deactivates faster.

Acknowledgements

The authors gratefully acknowledge the valuable comments and suggestions made by N. Marquez, MSc, and Dr. P. Kooyman. This work has been carried out through the financial support of Shell Global Solutions and Albemarle Catalyst Corporation.

References

[1] WHO, Air Quality Guidelines, WHO, 2000.
[2] Y. Kidoguchi, C. Yang, R. Kato, K. Miwa, JSAE Rev. 21 (2000) 469–475.
[3] T.C. Zannis, D.T. Hountalas, J. Energy Inst. 77 (2004) 16–25.
[4] F. Cignoli, S. De Iuliis, G. Zizak, Fuel 80 (2001) 945–955.
[5] A. Suchanek, ACS Div. Petrol Chem. Prep. 41 (1996) 583–584.
[6] B.H. Cooper, B.B.L. Donnis, Appl. Catal. A: Gen. 137 (1996) 203–223.
[7] B.H. Cooper, P. Sogaard-Anderson, P. Nielsen-Hannerup, M.C. Oballa, S.S. Shih, Catalytic Hydroprocessing of Petroleum and Distillates, Marcel Dekker, New York, 1994, pp. 279–290.
[8] A. Stanislaus, B.H. Cooper, Catal. Rev. Sci. Eng. 36 (1994) 75–123.
[9] N. Tsubaki, U.T. Turaga, C. Song, M. Misono, Catal. Today 104 (2005) 1–11.
[10] C. Song, X. Ma, Appl. Catal. B: Environ. 41 (2003) 207–238.
[11] S.A. Ali, M.A.B. Siddiqui, React. Kinet. Catal. Lett. 61 (1997) 363–368.
[12] R.G. Tailleur, J. Ravigli, S. Quenza, N. Valencia, Appl. Catal. A: Gen. 282 (2005) 227–235.
[13] H.R. Reinhoudt, R. Troost, A.D. van Langeveld, S.T. Sie, J.A.R. van Veen, J.A. Moulijn, Fuel Process. Technol. 61 (1999) 133–147.
[14] Y. Yoshimura, M. Toba, T. Matsui, M. Harada, Y. Ichihashi, K.K. Bando, H. Yasuda, H. Ishihara, Y. Morita, T. Kameoka, Appl. Catal. A: Gen. 322 (2007) 152–171.
[15] H. Yasuda, T. Kameoka, T. Sato, N. Kijima, Y. Yoshimura, Appl. Catal. A: Gen. 185 (1999) 199–201.
[16] R.M. Navarro, B. Pawelec, J.M. Trejo, R. Mariscal, J.L.G. Fierro, J. Catal. 189 (2000) 184–194.
[17] L. Le Bihan, Y. Yoshimura, Fuel 81 (2002) 491–494.
[18] S. Jongpatiwut, Z. Li, D.E. Resasco, W.E. Alvarez, E.L. Sughrue, G.W. Dodwell, Appl. Catal. A: Gen. 262 (2004) 241–253.
[19] E. Guillon, J. Lynch, D. Uzio, B. Didillon, Catal. Today 65 (2001) 201–208.

[20] K. Ito, K. Satoh, T. Tomino, M. Miyake, M. Ohshima, H. Kurokawa, K. Sugiyama, H. Miura, J. Jpn. Pet. Inst. 46 (2003) 315–321.
[21] E. Guillon, B. Didillon, D. Uzio, Oil Gas Sci. Technol.-Revue De L Institut Francais Du Petrole 61 (2006) 405–413.
[22] J.L. Rousset, L. Stievano, F. Aires, C. Geantet, A.J. Renouprez, M. Pellarin, J. Catal. 202 (2001) 163–168.
[23] H. Yasuda, N. Matsubayashi, T. Sato, Y. Yoshimura, Catal. Lett. 54 (1998) 23–27.
[24] T.-B. Lin, C.-A. Jan, J.-R. Chang, Ind. Eng. Chem. Res. 34 (1995) 4284–4289.
[25] I.R. Galindo, J.A. de Los Reyes, Fuel Process. Technol. 88 (2007) 859–863.
[26] A. Niquille-Rothlisberger, R. Prins, Catal. Today 123 (2007) 198–207.
[27] B. Pawelec, P. Castaño, J.M. Arandes, J. Bilbao, S. Thomas, M.A. Pena, J.L.G. Fierro, Appl. Catal. A: Gen. 317 (2007) 20–33.
[28] K.K.A. Rashid, K.V. Lakshmi, M. Nandan, K.O. Xavier, B. Sen, Recent Adv. Basic Appl. Aspects Ind. Catal. 113 (1998) 829–834.
[29] M. Saeys, J.W. Thybaut, M. Neurock, G.B. Marin, Mol. Phys. 102 (2004) 267–272.
[30] P. Castaño, J.M. Arandes, B. Pawelec, J.L.G. Fierro, A. Gutierrez, J. Bilbao, Ind. Eng. Chem. Res. 46 (2007) 7417–7425.
[31] P.A. Rautanen, M.S. Lylykangas, J.R. Aittamaa, A.O.I. Krause, Ind. Eng. Chem. Res. 41 (2002) 5966–5975.
[32] M.S. Lylykangas, P.A. Rautanen, A.O.I. Krause, Ind. Eng. Chem. Res. 41 (2002) 5632–5639.
[33] P. Castaño, B. Pawelec, J.L.G. Fierro, J.M. Arandes, J. Bilbao, Appl. Catal. A: Gen. 315 (2006) 101–113.
[34] T.H. DeFries, R.V. Kastrup, D. Indritz, Prediction of Cetane Number by Group Additivity and Carbon-13 Nuclear Magnetic Resonance, 1987, pp. 188–193.
[35] S. Sato, Y. Sugimoto, K. Sakanishi, I. Saito, S. Yui, Fuel 83 (2004) 1915–1927.
[36] T.C. Huang, B.C. Kang, Ind. Eng. Chem. Res. 34 (1995) 1140–1148.
[37] S. Toppinen, T. Salmi, T.K. Rantakyla, J. Aittamaa, Ind. Eng. Chem. Res. 36 (1997) 2101–2109.
[38] T. Fujikawa, K. Idei, K. Ohki, H. Mizuguchi, K. Usui, Appl. Catal. A: Gen. 205 (2001) 71–77.
[39] M.R. Riazi, J.H. Vera, Ind. Eng. Chem. Res. 44 (2005) 186–192.
[40] M.R. Riazi, Y.A. Roomi, Chem. Eng. Sci. 62 (2007) 6649–6658.
[41] L.J. Florusse, C.J. Peters, J.C. Pamies, L.F. Vega, H. Meijer, AIChE J. 49 (2003) 3260–3269.
[42] C.H. Bartholomew, Appl. Catal. A: Gen. 212 (2001) 17–60.
[43] C.H. Bartholomew, P.K. Agrawal, J.R. Katzer, Adv. Catal. 31 (1982) 135–242.
[44] G.F. Froment, K.B. Bischoff, Chem. Eng. Sci. 16 (1961) 189–201.
[45] N.M. Ostrovskii, Chem. Eng. J. 120 (2006) 73–82.
[46] C. Satterfield, Mass Transfer in Heterogeneous Catalysis, MIT Press, Cambridge, MA, 1970.
[47] S.R. Vatcha, D.B. Dadyburjor, Ind. Eng. Chem. Process Des. Dev. 25 (1986) 229–236.
[48] J.-R. Chang, S.L. Chang, T.-B. Lin, J. Catal. 169 (1997) 338–346.
[49] S. Toppinen, T.K. Rantakyla, T. Salmi, J. Aittamaa, Ind. Eng. Chem. Res. 35 (1996) 4424–4433.
[50] M.S. Lylykangas, Kinetic Modeling of Liquid-Phase Hydrogenation Reactions, Department of Chemical Technology, Helsinki University of Technology, Helsinki, 2004, p. 23.
[51] S.R. Kirumakki, B.G. Shpeizer, G.V. Sagar, K.V.R. Chary, A. Clearfield, J. Catal. 242 (2006) 319–331.